

Identifying reliable periods in 2MASS J09213414-5939068, IGR J16167-4957, and V667 Pup

Arti Joshi^{1*}

Institute of Astrophysics, Pontificia Universidad Católica de Chile, Av. Vicuña MacKenna 4860, 7820436, Santiago, Chile

January 30, 2024

ABSTRACT

Detailed timing analyses of three cataclysmic variables, namely 2MASS J09213414-5939068, IGR J16167-4957, and V667 Pup are carried out using the long-baseline and high-cadence optical photometric data from the Transiting Exoplanet Survey Satellite (*TESS*). Periods of 908.12 ± 0.05 s and 990.10 ± 0.06 s are observed in the optical variation of 2MASS J09213414-5939068 that were not found in earlier studies and appear to be probable spin and beat periods of the system, respectively. The presence of multiple periods at spin, beat, and other sidebands indicates that 2MASS J09213414-5939068 likely belongs to an intermediate polar class of magnetic cataclysmic variables that seems to be accreted via a disc-overflow mechanism. Clear evidence of a period of 582.45 ± 0.04 s is found during the *TESS* observations of IGR J16167-4957, which can be interpreted as the spin period of the system. Strong modulation at this frequency supports its classification as an intermediate polar, where accretion may primarily be governed by a disc. The dominance of the spin pulse unveils the disc-fed dominance accretion in V667 Pup, but the detection of the previously unknown beat period of 525.77 ± 0.03 s suggests that a portion of the material is also accreted through a stream. Moreover, the double-peaked structure observed in the optical spin pulse profile of V667 Pup suggests the possibility of a two-pole accretion geometry, where each pole accretes at a different rate and is separated by 180° .

Key words. accretion, accretion discs – novae, cataclysmic variables – stars: individual: (2MASS J09213414-5939068, IGR J16167-4957, V667 Pup) – stars: magnetic field.

1. Introduction

Cataclysmic variables (CVs) are semi-detached binary systems in which a primary white dwarf (WD) accretes material from a Roche-lobe-filling late-type secondary star. When the WD magnetic field is $< 10^6$ G, the material transferred from the secondary flows through the inner Lagrangian point and orbits the primary, forming an accretion disc (Warner 1995). However, when the WD is highly magnetised ($\sim 10^{6-9}$ G), the accretion disc is either fully (Cropper 1990, e.g. known as AM Herculis; a polar) or partially disrupted (Patterson 1994, e.g., known as DQ Herculis; an intermediate polar (IP)).

The magnetic field strength of the WD plays a vital role in controlling the motion of the accretion flow within the effective magnetospheric radius. In IPs, the magnetic field strength of the WD (typically less than 10^7 G) causes the accreting material to form an accretion disc. However, at a certain point, the magnetic pressure exceeds the ram pressure, leading to the disruption of the disc. The material then flows along the magnetic field lines. The matter in the accretion column impacts the poles of WDs with supersonic velocities, which leads to the formation of strong shocks that emit cyclotron (optical/infrared) and thermal bremsstrahlung (X-ray) radiation (Aizu 1973). The majority of the IPs peaks at the hard luminosity of $10^{33}-10^{34}$ erg s^{-1} , but there is also evidence of low-luminosity IPs. These are mostly shorter-period systems below the period gap of 2-3 h, and they have a luminosity of $\sim 10^{30}-10^{32}$ erg s^{-1} (Schwope 2018; de Martino et al. 2020).

Intermediate polars are asynchronous systems, where the spin period (P_ω) of the WD is typically shorter than the orbital period (P_Ω) of the binary system. The optical and X-ray signals in IPs are modulated on the spin period, orbital period, beat period ($P_{\omega-\Omega}$), and other sidebands. The multiple periodicities in the X-ray and optical bands is a distinguishing feature of these systems and are caused by intricate interactions between the spin and orbital modulations, either as a result of changes in the accretion rate or as a result of the reprocessing of primary radiation by other components of the system. Thus, an essential diagnostic tool for establishing the IP nature of a possible member of this class are multiple periodic components. Moreover, three different accretion mechanisms are thought to occur in IPs: disc-fed, stream-fed (disc-less), and disc-overflow. These mechanisms depend upon the magnetic field strength of the WD, on the mass accretion rate, and on the binary orbital separation. In these scenarios, the mode of accretion can be identified through the orbital, spin, beat, and sideband frequencies. In disc-fed accretion, the inner edge of the accretion disc is truncated at the magnetospheric radius, which results in the formation of so-called accretion curtains near the magnetic poles of the WD (Rosen et al. 1988). A strong modulation occurs at the spin frequency of the WD in disc-fed accretion (Kim & Beuermann 1995; Norton et al. 1996). In the disc-less or stream-fed accretion, the high magnetic field of the WD prevents the formation of a disc, and infalling material flows along the magnetic field lines to the pole caps (Hameury et al. 1986). Modulation at the beat frequency (Hellier 1991; Wynn & King 1992) is a true indicator of disc-less accretion. According to Wynn & King (1992), an asymmetry between the magnetic poles can also lead to a modulation at

* E-mail: ajoshi@astro.puc.cl, aartijoshiphysics@gmail.com

Table 1. Log of the *TESS* observations with start and end times in calendar date.

Object	Sector	Start Time	End Time	Total observing days
2MASS J09213414–5939068	09	2019-02-28T18:08:25.5	2019-03-25T23:26:48.1	25.2
	10	2019-03-26T22:30:47.7	2019-04-22T04:22:31.0	26.2
IGR J16167–4957	12	2019-05-21T11:52:43.3	2019-06-18T09:30:37.7	27.9
V667 Pup	34	2021-01-14T06:29:54.5	2021-02-08T13:39:26.4	25.2

the spin frequency in addition to the beat frequency when accretion occurs via the accretion stream. Then the $2\omega - \Omega$ frequency in X-rays significantly contributes to confirming the accretion mode as stream-fed, along with the sometimes dominant Ω component, $\omega - \Omega$, and ω . In the disc-overflow accretion (Lubow 1989; Armitage & Livio 1996), a combination of both disc-fed and stream-fed accretions can occur, but a part of the accretion stream skips the disc and directly interacts with the WD magnetosphere (Hellier et al. 1989; King & Lasota 1991). Modulations at both spin and beat frequencies are expected to occur, and the main difference lies in the varying power and amplitude between the two (Hellier 1991, 1993).

In this paper, I present detailed optical analyses of three CVs, namely, 2MASS J09213414–5939068, IGR J16167–4957, and V667 Pup. The light-curve morphologies, spin period, other sideband periods, and the specific classification of 2MASS J09213414–5939068 are still unknown. They are essential for investigating the nature of this system, however. Moreover, the absence of a spin signal in IGR J16167–4957 and the lack of beat modulation in V667 Pup led to revisit their properties, which are vital for revealing the exact nature and mode of accretion in these systems. I therefore present precise and uninterrupted long *TESS* optical observations to unveil the nature of these systems. A summary of the available information for these sources is given below.

2MASS J09213414–5939068 (hereafter J0921) was selected as a CV based on the detection of $H\alpha$ emission (Pretorius & Knigge 2008). Pretorius & Knigge (2008) spectroscopic studies revealed a strong He II ($\lambda 4686 \text{ \AA}$) emission line, as well as the Balmer and He I emission lines, overlaid on a blue continuum. However, photometric observations exhibited no modulations other than flickering. Based on time-resolved spectroscopic data, a period of $3.041 \pm 0.009 \text{ hr}$ was determined and assumed to be the orbital period of the system.

IGR J16167–4957 (hereafter J1616) was discovered as a hard X-ray source by Barlow et al. (2006), and (Tomsick et al. 2006) concluded it was not one of the high-mass X-ray binaries. It was identified as a CV by Masetti et al. (2006) based on the optical spectral features. Later, Pretorius (2009) determined its orbital period as $5.004 \pm 0.005 \text{ hr}$ using the time-resolved spectroscopic observations. The orbital period was not detected in their high-speed photometric observations. A signal of approximately 585 s was observed for half of the observing time for the one-epoch light curve, but it was absent in their other observational epochs, leading them to hypothesise that it might be a quasi-periodic signal. Subsequently, the Rossi X-ray Timing Explorer (*RXTE*) spectrum led to the suggestion that J1616 is likely to be classified as an IP (Butters et al. 2011). The lack of an X-ray spin period and a period of 585 s means that its status as an unclassified system remains, however.

V667 Pup has frequently been mentioned in the Astronomer’s Telegrams over the course of several months early in 2006. It was first identified as a CV by Ajello et al. (2006)

based on Neil Gehrels Swift Observatory (*Swift*) observations. Masetti et al. (2006) identified two nearby objects, the brighter of which exhibited a spectrum typical of a normal G/K type Galactic star. However, the fainter object was identified as the true optical counterpart with the detection of spectral features, including emission lines of $H\alpha$, $H\beta$, He I ($\lambda 5875 \text{ \AA}$), and He II ($\lambda 4686 \text{ \AA}$). These signatures were concluded to be those of an accretion disc in a low-mass X-ray binary. Later, Patterson et al. (2006) reported a stable spin pulsation at a period of $\sim 512.4 \text{ s}$ using optical photometry and classified it as an IP. The optical counterpart of V667 Pup was further observed by Marsh et al. (2006), who detected spin pulsations identical to those found by Patterson et al. (2006). In the same year, Torres et al. (2006) reinforced its classification as a probable IP with the detection of Balmer emission lines from $H\alpha$ to $H\gamma$, including He II ($\lambda 4686 \text{ \AA}$), He I ($\lambda 5876 \text{ \AA}$), He I ($\lambda 6678 \text{ \AA}$), and the Bowen blend in emission. Upon revisiting the *Swift* data, Wheatley et al. (2006) detected an X-ray pulsation consistent with the proposed spin period of $\sim 512 \text{ s}$. Based on radial velocity measurements of the $H\alpha$ emission lines, Thorstensen et al. (2006) derived an orbital period of $5.604 \pm 0.019 \text{ hr}$, which was subsequently refined by Thorstensen & Halpern (2013) as $5.611 \pm 0.005 \text{ hr}$. Butters et al. (2007) reported an X-ray spin period of $512.4 \pm 0.3 \text{ s}$ based on the *RXTE* observations, which supported the classification of this object as an IP. Later, precise photometric measurements of this object were reported by Thorstensen & Halpern (2013), who revealed fluctuations of about 0.05 mag for V667 Pup, while the companion exhibited somewhat smaller variations. Moreover, their observed spectrum revealed relatively weak emission lines; He II ($\lambda 4686 \text{ \AA}$) displayed a strength that was comparable to that of the $H\beta$ emission line. At a period of 5.61 hr, their analysis revealed a prominent modulation in the $H\alpha$ emission line velocities.

The paper is organised as follows: The observations and data reduction are summarised in the next section. Section 3 contains analyses and the results. Finally, the discussion and conclusions are presented in Sections 4 and 5, respectively.

2. Observations and data reduction

The archival data used in this study were obtained from observations by *TESS* for all three systems. *TESS* has four small telescopes with four cameras with a field-of-view of $24 \times 24 \text{ degree}^2$ each, which are aligned to cover $24 \times 96 \text{ degree}$ strips of the sky called ‘sectors’ (see Ricker et al. 2015, for details). The *TESS* bandpass covers the wavelength range from 600 nm to 1000 nm, with an effective wavelength of 800 nm. A detailed log for the *TESS* observations of all three sources is given in Table 1. The data are available at the Mikulski Archive for Space Telescopes (MAST) data archive¹ with the identification numbers TIC 387201824, TIC 411381210, and TIC 750058684 for J0921,

¹ <https://mast.stsci.edu/portal/Mashup/Clients/Mast/Portal.html>

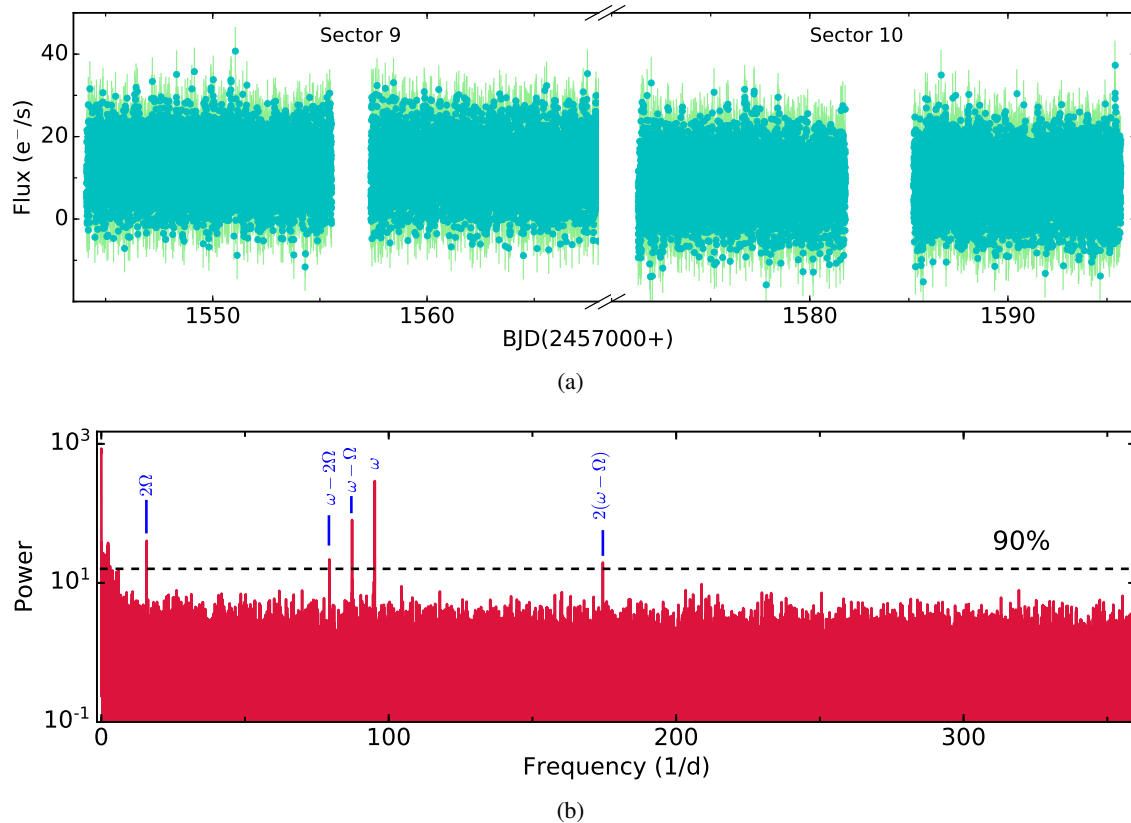


Fig. 1. (a) *TESS* light curves of J0921 to reveal the brightness variations in sectors 9 and 10, while (b) LS power spectrum obtained from the combined *TESS* observations of sectors 9 and 10. The significant frequencies observed in the power spectrum lie above the 90% confidence level (represented by the dashed horizontal black line) and are marked.

J1616, and V667 Pup, respectively. The cadence for each source was 2 min. The *TESS* pipeline provides two flux values: simple aperture photometry (SAP), and pre-search data-conditioned SAP (PDCSAP). The PDCSAP light curve attempts to remove instrumental systematic variations by fitting and removing the signals that are common to all stars on the same CCD². By employing this approach, aperiodic variability might be removed from the data. PDCSAP also corrects for the amount of flux captured by the photometric aperture and for crowding from known nearby stars, while SAP does not. To confirm that the PDCSAP data retain all aperiodic variability, a periodogram analysis was performed on all sources, considering both SAP and PDCSAP data. The PDCSAP and SAP light curves both showed the same short-period variability, indicating that the PDCSAP data are reliable and can be used for the further analysis. Anomalous event-related data displayed quality flags above 0 in the FITS file structure, and I therefore selected only the data with a QUALITY flag = 0.

3. Analysis and results

3.1. 2MASS J09213414–5939068

The *TESS* light curves of J0921 for sectors 9 and 10 are shown in Figure 1a. To search for the periodicity, a period analysis was conducted using the Lomb-Scargle (LS) periodogram algorithm (Lomb 1976; Scargle 1982). The LS power spectrum obtained

² see section 2.1 of the *TESS* archive manual available at <https://outerspace.stsci.edu/display/TESS/2.0+-+Data+Product+Overview>

from the combined *TESS* observations of both sectors is shown in Figure 1b, where the positions of all identified frequencies are marked. The power spectrum displays a prominent peak that corresponds to a period of ~ 908 s, which can be assigned as the spin period of the WD. The other significant peak at about a period of 1.5 hr corresponds to the second harmonic of the orbital period, precisely half of the orbital period of ~ 3.04 hr, as determined by Pretorius & Knigge (2008). When I consider ~ 908 s and ~ 3.04 hr as the spin and orbital periods, respectively, the derived period at ~ 990 s can be interpreted as the beat period of the system. The other identified periods correspond to the frequencies $\omega - 2\Omega$ and $2(\omega - \Omega)$. These observed frequencies exhibit lower power values than the ω frequency. The significance of these detected peaks is determined by calculating the false-alarm probability (see Horne & Baliunas 1986). The dashed horizontal black line represents the 90% confidence level. Periods corresponding to these dominant peaks are also derived from sectors 9 and 10 separately. They are well consistent with the periods derived from the combined *TESS* data and are given in Table 2. Based on the exceptionally long baseline provided by *TESS*, the temporal evolution of the power spectra was also examined in successive one-day intervals. The data were segmented from each sector into successive intervals of one day. As a result, sectors 9 and 10 have a total of 24 and 22 data segments, respectively. Furthermore, the LS periodogram analysis was performed on each one-day dataset. Figures 2a and 2b exhibit one-day incremented trailed power spectra for sectors 9 and 10, respectively. The frequencies 2Ω , $\omega - \Omega$, and ω are irregular throughout the time-resolved power spectra and are sometimes significant and sometimes below the confidence level. In

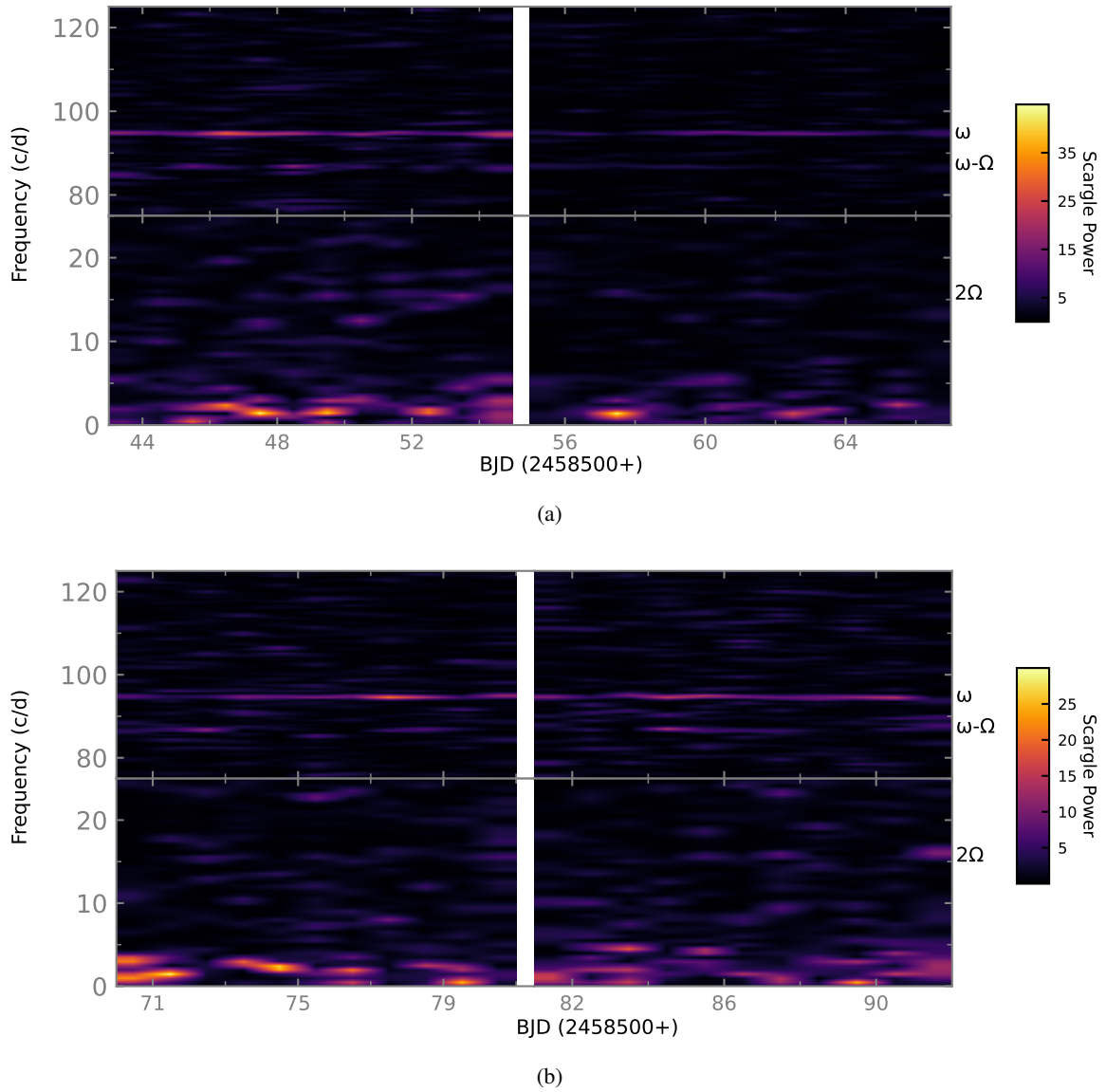


Fig. 2. One-day time-resolved *TESS* power spectra of J0921 near the 2Ω and ω frequency region for (a) sector 9 and (b) sector 10.

Table 2. Periods corresponding to dominant peaks in the LS power spectra of J0921, J1616, and V667 Pup.

Object	Sector	Periods						
		P_{Ω} (hr)	$P_{2\Omega}$ (hr)	$P_{(\omega-2\Omega)}$ (s)	$P_{(\omega-\Omega)}$ (s)	P_{ω} (s)	$P_{2\omega}$ (s)	$P_{2(\omega-\Omega)}$ (s)
J0921	9	..	1.518 ± 0.001	1088.80 ± 0.14	990.21 ± 0.12	907.98 ± 0.11	..	495.13 ± 0.03
	10	..	1.518 ± 0.001	1088.79 ± 0.14	990.25 ± 0.12	908.01 ± 0.11	..	495.11 ± 0.03
	Combined [†]	..	1.519 ± 0.001	1088.96 ± 0.07	990.10 ± 0.06	908.12 ± 0.05	..	495.10 ± 0.01
J1616	12	4.99 ± 0.01	582.45 ± 0.04
V667 Pup	34	5.58 ± 0.01	2.79 ± 0.01	..	525.77 ± 0.03	512.40 ± 0.03	256.19 ± 0.01	..

[†] represents the periods derived from the combined *TESS* data of sectors 9 and 10.

contrast to the combined power spectrum, no significant $\omega - 2\Omega$ and $2(\omega - \Omega)$ signals are detected during one-day observations of either sector.

The periodic variability of J0921 was also inspected by folding the light curves over the spin and orbital periods and using the first point of the *TESS* observation as the reference epoch,

BJD = 2458544.114307. Spin and orbital phase-folded light curves were obtained with a binning of 20 points in a phase along with the best-fit sine function and with the sum of two best-fit functions, a sine and a cosine, respectively. They are shown in Figure 3. Clear periodic sinusoidal modulations are observed in the spin-phase-folded light curve, whereas the orbital-phase-

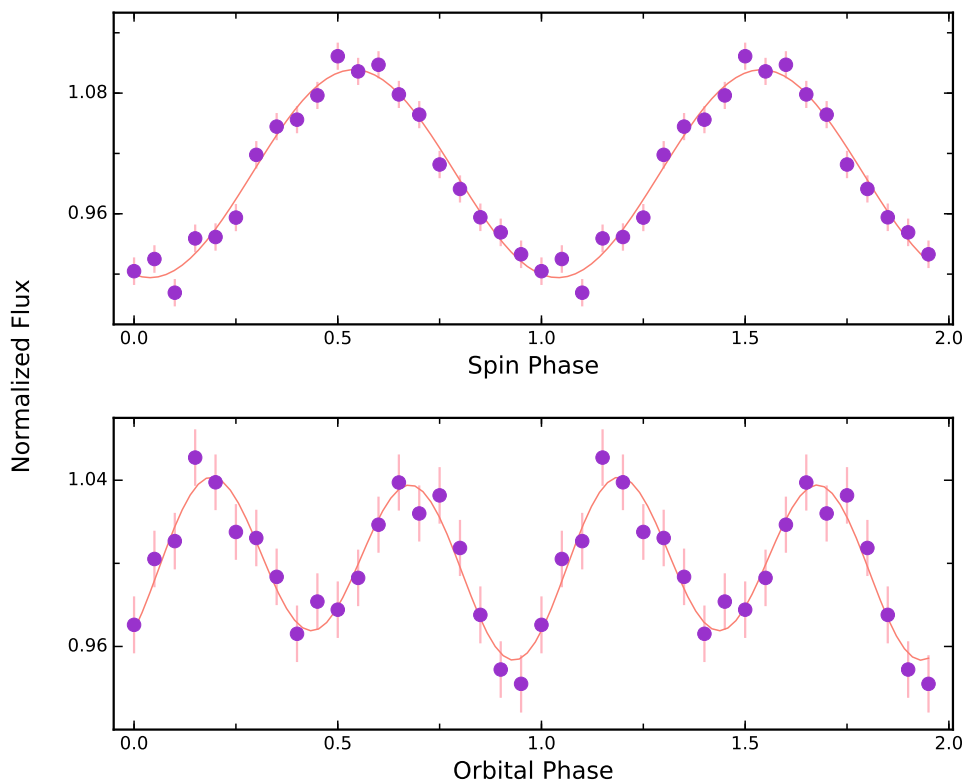


Fig. 3. Spin (top) and orbital (bottom) phase-folded *TESS* light curves of J0921 obtained from the combined data of sectors 9 and 10.

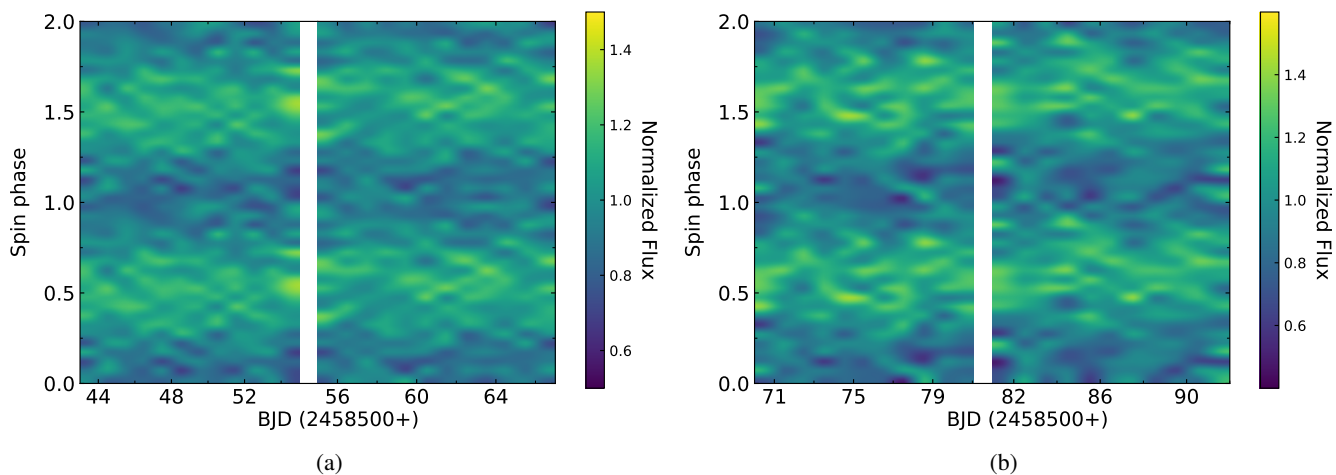


Fig. 4. Evolution of the spin-pulse profiles during one-day *TESS* observations of J0921 for (a) sector 9 and (b) sector 10.

folded light curve exhibits double-peaked modulations. This is also evident from the power spectrum, which reveals a strong significant peak at the second harmonic of the orbital period. Furthermore, to show the evolution of the short-term variations, the day-wise periodic variation during the rotation of the WD was explored. Following the same approach as mentioned above, each day's light curve was folded with a binning of 20 points in a phase. Figures 4a and 4b represent the colour-composite plots for the one-day spin-phased pulse profile for sectors 9 and 10, respectively. Strong single broad-peak spin modulations are observed throughout the one-day *TESS* observations in both sectors.

3.2. *IGR J16167–4957*

Figure 5a displays the complete *TESS* light curve of J1616, showing short-term fluctuations superimposed on long-term variability upon careful examination. In order to identify the periodicities, the LS periodogram analysis was performed on the entire *TESS* dataset, which is shown in Figure 5b, where the positions of the two identified frequencies are marked. Both periods are observed above the 90% confidence level. The detected significant frequency corresponds to the orbital period of 4.99 ± 0.01 hr and confirms previous results of Pretorius (2009). Another significant peak corresponds to the period of 582.45 ± 0.04 s and can be considered as the spin period of the WD in J1616. The dominance of spin modulation over orbital modulation is clearly

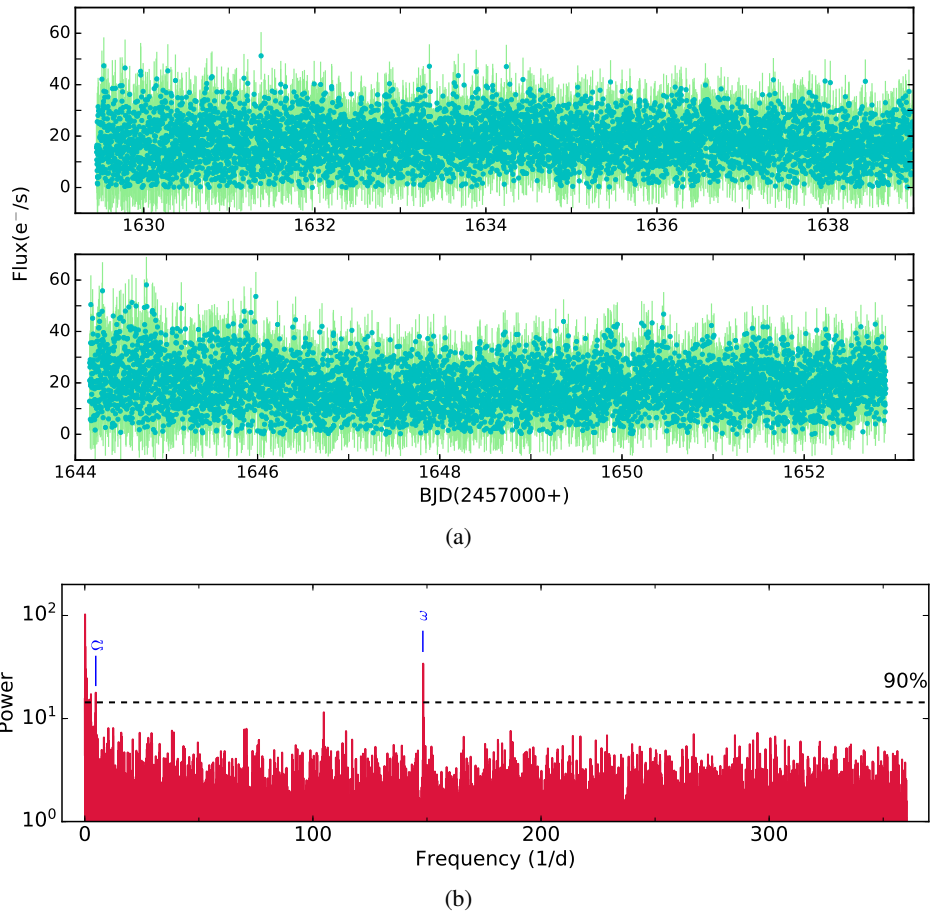


Fig. 5. (a) *TESS* light curve to reveal the brightness variations in J1616, and (b) LS power spectrum obtained from the *TESS* observations of J1616. The significant frequencies observed in the power spectrum lie above the 90% confidence level (represented by the dashed horizontal black line) and are marked.

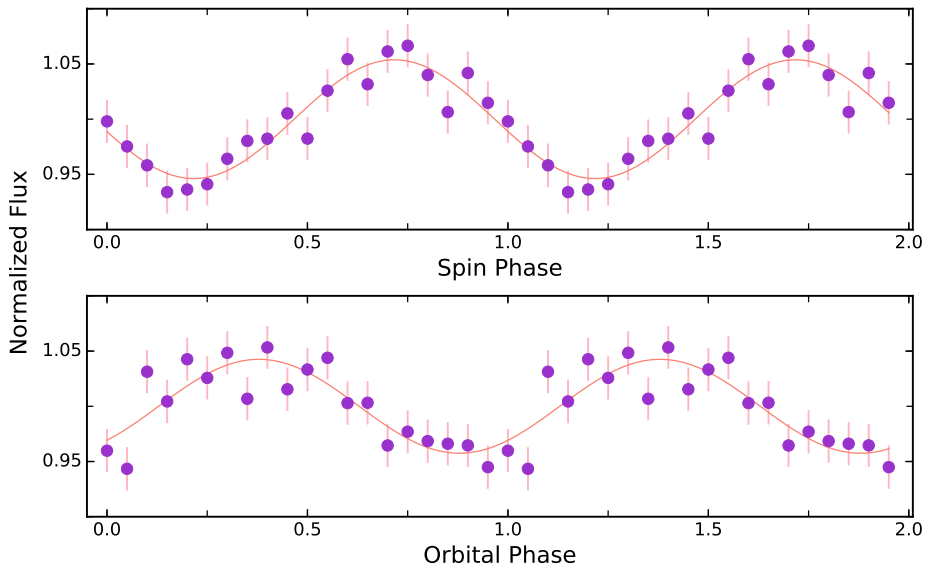


Fig. 6. Spin (top) and orbital (bottom) phase-folded *TESS* light curves of J1616.

visible in its power spectrum. Moreover, a cluster of frequencies in the lower-frequency region of 0.1 and 0.3 c/d is also present in the power spectrum and is apparently unrelated to the frequencies identified in the J1616 power spectrum. Similar to J0921, a one-day time-resolved power spectrum analysis was also con-

ducted for J1616. Unfortunately, the spin and orbital frequencies were both detected below the confidence level throughout each day-segment power spectrum.

To study the phased-light curve variations, the *TESS* light curve was folded using the zero time of the first *TESS* obser-

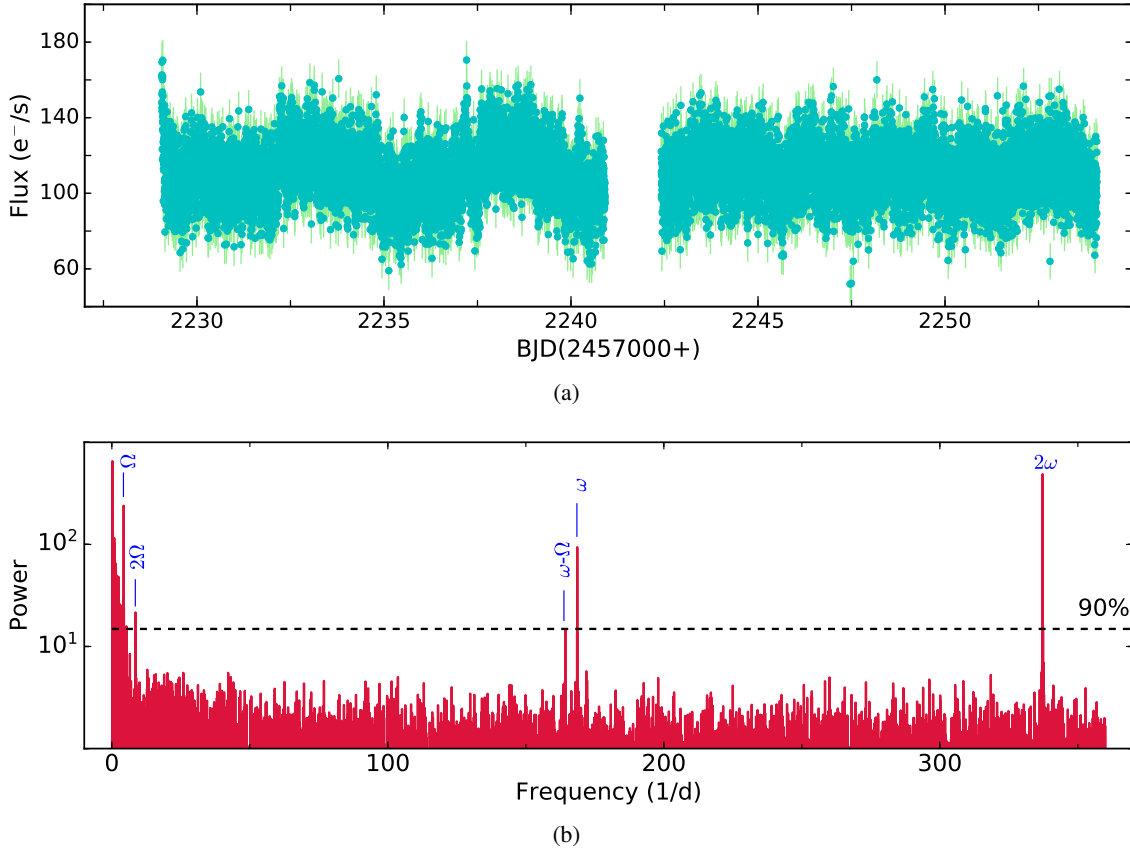


Fig. 7. (a) *TESS* light curve to reveal the brightness variations in V667 Pup, and (b) LS power spectrum obtained from the *TESS* observations of V667 Pup. The significant frequencies observed in the power spectrum lie above the 90% confidence level (represented by the dashed horizontal black line), and are marked.

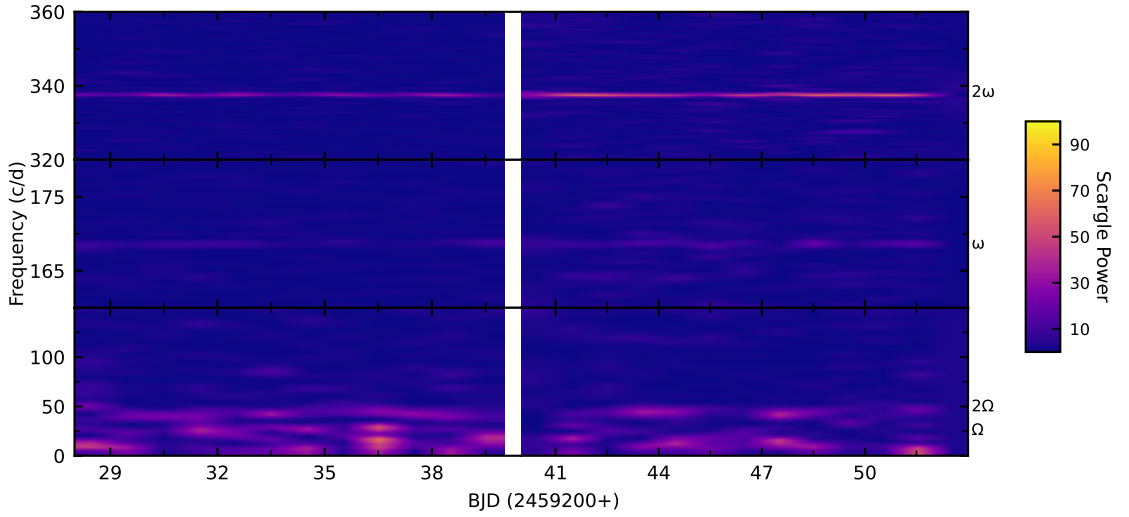


Fig. 8. One-day time-resolved *TESS* power spectrum of V667 Pup near the Ω , ω , and 2ω frequency regions.

variation, BJD=2458629.446496, and the derived orbital and spin periods. The light curves were folded with a binning of 20 points in a phase, and they are shown in Figure 6. The orbital and spin-phase-folded light curves exhibit sinusoidal modulations, and broad peaks occur in phases ~ 0.35 and ~ 0.75 , respectively.

3.3. V667 Pup

Figure 7a shows the *TESS* light curve of V667 Pup, where the variable nature of the source is evident. To probe the periodic nature of V667 Pup, the LS periodogram analysis was performed on the combined *TESS* timing data. It is shown in Figure 7b. Two fundamental periods at 5.58 ± 0.01 hr and 512.40 ± 0.03 s are observed in the LS power spectrum. They correspond to the or-

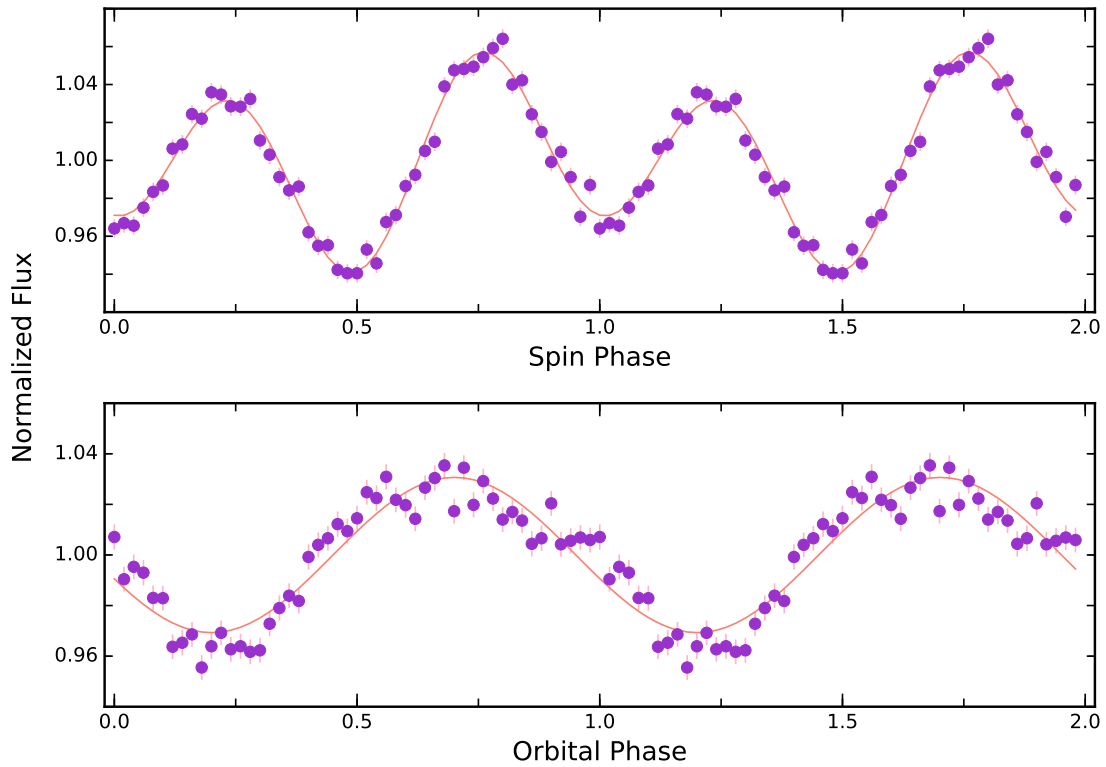


Fig. 9. Spin (top) and orbital (bottom) phase-folded *TESS* light curves of V667 Pup.

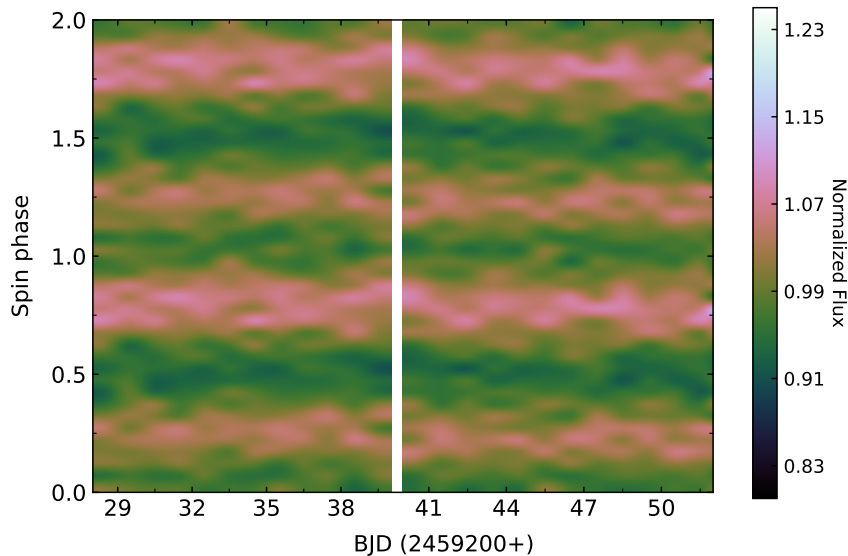


Fig. 10. Evolution of the spin-pulse profiles during one-day *TESS* observations of V667 Pup.

bital and spin periods of the system, respectively. The frequency corresponding to the period of 525.77 ± 0.03 s is also present in the power spectrum and can be attributed to the beat period of the system, which was not detected in the earlier observations. All detected peaks lie above the 90% confidence level. All the derived periods corresponding to five significant peaks at frequencies Ω , 2Ω , $\omega - \Omega$, ω , and 2ω are given in Table 2. Similar to J0921, the evolution of the power spectra was also inspected in consecutive one-day time segments. The trailed LS power spectra with one-day increments are shown in Figure 8. Each day-segment exhibits strong power only in the detected significant 2ω frequency. However, the ω and Ω frequencies are sporadic

throughout the time-resolved power spectra. No significant 2Ω and $\omega - \Omega$ frequencies are detected in one-day power spectra, however.

The *TESS* light curves were folded using the same reference epoch as given by Thorstensen & Halpern (2013) in units of BJD as 2453812.7598 and more precise spin and orbital periods derived from the *TESS* observations (see Table 2). The spin (along with the sum of two best-fit functions, a sine and a cosine) and orbital (along with a best-fit sine function) phase-folded light curves with a phase bin of 0.02 are shown in Figure 9. The *TESS* light curves reveal two prominent peaks during a rotation of the WD, where the amplitude of the first peak is slightly smaller

than that of the second peak. However, a single broad hump is seen during half of the orbital cycle of V667 Pup. A similar behaviour of a double-peaked spin-pulse profile is also observed in the one-day *TESS* observations, as depicted in Figure 10.

4. Discussion

Detailed time-resolved analyses were carried out for three CVs, J0921, J1616, and V667 Pup, using high-cadence optical photometric data from the *TESS*. I speculate that J0921 belongs to the IP class of magnetic CVs that accrete with the disc-overflow mechanism, whereas the detection of a spin signal in J1616 and a beat signal in V667 Pup supports the classification of these systems as IPs, where accretion may primarily be governed by disc-fed and disc-overflow mechanisms, respectively.

In the optical data from the *TESS*, five significant periods were observed in J0921, including a fundamental period of 908.12 ± 0.05 s, which is probably the spin period of the WD. Considering ~ 908 s and ~ 3.04 hr as spin and orbital periods, respectively, I estimated the beat period to be ~ 990 s, which is also present in the power spectrum of J0921. The presence of these frequencies indicates that J0921 may belong to the IP class of magnetic CVs. The dominant peak at the 2Ω frequency may suggest a strong contribution from the secondary star due to ellipsoidal modulation. The combinations of spin and orbital frequencies are typically considered the primary frequency components in the search for a possible accretion mechanism in IPs. In this context, the detection of $\omega - \Omega$ in J0921 seems intrinsic and provides indications that there would be material flow with an accretion stream. This modulation is not entirely caused by the amplitude modulation of the spin frequency at the orbital period: If it were the orbital modulation of the ω frequency, then $\omega + \Omega$ should be present in the power spectrum with the same power as $\omega - \Omega$, which is not observed in our data. Moreover, the origin of the $\omega - 2\Omega$ frequency cannot be due to the modulation of ω at 2Ω ; otherwise, $\omega + 2\Omega$ should also be present in the power spectrum. The simultaneous presence of $\omega - 2\Omega$ along with the $\omega - \Omega$ frequency confirms that the origin of $\omega - 2\Omega$ is due to the orbital modulation of the $\omega - \Omega$ component ($\omega - \Omega \pm \Omega = \omega - 2\Omega$ and ω), as was pointed out by Warner (1986).

The detection of $\omega - \Omega$ along with strong ω indicates that J0921 may accrete via a combination of disc and stream. Additionally, one-day time-resolved power spectra revealed fluctuations in the significant powers of ω and $\omega - \Omega$. In sector 10, particularly on day 73, the power of $\omega - \Omega$ is notably higher than the power of ω , indicating the dominance of stream-fed accretion. However, for the remaining observations, the power associated with $\omega - \Omega$ is either undetected or is relatively lower than ω , which suggests that J0921 likely accretes predominantly through the disc or accretes via the disc-overflow mechanism with disc-fed dominance. The observed change may be attributed to variations in both the mass accretion rate and the activity of the secondary star. In earlier studies, the alterations in the accretion mechanism were also investigated by examining the power spectra of IPs, focusing on the influence of the spin and beat frequency (Buckley & Tuohy 1989; Norton et al. 1997; Littlefield et al. 2020; Rawat et al. 2021). Thus, a variable disc-overflow accretion may be one of the possible accretion mechanisms during the *TESS* observations of J0921. Alternatively, Murray et al. (1999) suggested that a spiral disc structure might give rise to modulations at orbital sidebands of the spin frequency in IPs, including a beat and its second harmonic. Moreover, Warner (1986) pointed out that the reprocessing of X-rays by structures stationary in the binary rest frame would yield an optical beat

signal in IPs. These could also provide alternative explanations for the detection of the beat signal in J0921.

For J1616, a significant period of 4.99 ± 0.01 hr is detected, which corresponds to the orbital period of the system. Due to the better time-cadence and longer-baseline of *TESS*, a clearly significant period of 582.45 ± 0.04 s is observed in its power spectrum. No clear detection of this period was observed previously by Pretorius (2009) and Butters et al. (2011). However, within the uncertainties, this 582 s signal may match the intermittent 585 s signal observed by Pretorius (2009). The detected period of 582.45 ± 0.04 s appears to be the probable spin period of the WD in J1616. Thus, the existence of dominant modulation at this frequency supports its classification as an IP. The IPs are generally united with three groups: slow rotators with $P_\omega/P_\Omega \sim 0.5$, intermediate rotators with $P_\omega/P_\Omega \sim 0.1$, and fast rotators with $P_\omega/P_\Omega \sim 0.01$. If the proposed spin period is indeed the actual period, then $P_\omega/P_\Omega \sim 0.03$ for J1616. Thus, with $P_\omega/P_\Omega \sim 0.03$ or $P_\omega \sim 582$ s, J1616 appears to belong to the fast-rotator category. With these values of the orbital and spin periods, the inferred value of $P_{\omega-\Omega}$ period is ~ 601.96 s, which corresponds to the frequency of ~ 143.5 c/d. No period corresponding to this frequency is detected in its power spectrum. The dominant ω and the absence of $\omega - \Omega$ or any other sideband frequency signifies that it might be a disc-fed accretor, however. Nevertheless, further follow-up X-ray observations are needed to better characterise the candidate spin signal and the accretion geometry of the system.

Five significant frequencies, Ω , 2Ω , $\omega - \Omega$, ω , and 2ω , are detected in the optical *TESS* power spectrum of V667 Pup. All the observed frequencies reinforce the IP nature of V667 Pup. Based on the longer baseline available with the *TESS* data, a refined spin period of 512.40 ± 0.03 s is detected. This derived spin period is found to be clearly consistent with the periods derived from previous measurements (see Patterson et al. 2006; Butters et al. 2007). The *TESS* data derived the orbital period of V667 Pup as 5.58 ± 0.01 hr, which is found to be somewhat inconsistent with the spectroscopic period of 5.611 ± 0.005 determined by Thorstensen & Halpern (2013). With $P_\omega/P_\Omega \sim 0.03$ and $P_\omega \sim 512$ s, V667 Pup also seems to belong to the category of fast rotators, similar to the other IPs, RX J2133.7+5107, V455 And, V418 Gem, and NY Lup. Along with the spin and orbital periods, the other observed frequencies can also serve as an important diagnostic to understand the mode of accretion in this system. Among them, a significant $\omega - \Omega$ frequency with a period of 525.77 ± 0.03 s is detected in the study of the V667 Pup for the first time. Similar to J0921, the presence of $\omega - \Omega$ seems intrinsic because $\omega + \Omega$ is not detected in its power spectrum, which safely affirms that the detection of the beat modulation is entirely intrinsic and originated from accretion through the stream. Although the strong ω and 2ω frequencies suggest the dominance of disc-fed accretion, however, the detection of an additional beat frequency implies that some fraction of material is also accreted via a stream. Therefore, V667 Pup is also likely to be a disc-overflow accreting intermediate polar.

The observed optical spin modulations in V667 Pup are non-sinusoidal compared to most IPs and exhibit a double-peaked pulse profile, as expected from the observed second harmonic of the spin pulse in the power spectrum, which can be interpreted in terms of two emitting poles. The relative contribution of the two poles to the observed emission can be explained based on the ratio of the fundamental-to-second harmonic amplitude. The amplitude of the first hump is found to be smaller than that of the second hump, and both peaks are separated by about 0.5 in phase, indicating that the two poles may accrete at a different rate and that they are separated by 180° . Based on the strength of the

magnetic field of the WD, Norton et al. (1999) suggested that the two-pole accretion model can describe the double-peaked profile structure in IPs. Their model predicts that weak magnetic fields are typical for short-period spinning IPs, which results in double-peaked pulse profiles. This might be one of the reasons that can explain the double-peaked optical pulse profile in the short-period rotating IP V667 Pup. Another possibility could be that the geometry allows the two opposite poles to come into view for the observer (e.g., V405 Aur Evans & Hellier 2004). This means that the geometry of the system might be such that at certain orientations, both poles (which are located on opposite sides of the system) are aligned in a way that they can be seen simultaneously by the observer. This alignment allows us to observe the distinct double-peaked pattern in the optical pulse. Other than the spin modulations, obscuration of the WD by the material rotating in the binary frame or an eclipse of the hotspot by an optically thick disc may cause the broad single-peaked orbital modulation in V667 pup.

5. Conclusions

The characteristics of J0921, J1616, and V667 Pup are summarised below.

1. J0921 is probably an intermediate polar with a detection of two periods at 908.12 ± 0.05 s and 990.10 ± 0.06 s, which are interpreted as the spin and beat periods, respectively. The detection of both $\omega - \Omega$ and ω suggests that J0921 is likely undergoing through the disc-overflow mechanism.
2. The detection of an unambiguous dominant period at 582.45 ± 0.04 s in J1616 can be interpreted as the spin period of the WD, which supports its classification as an IP, where accretion may primarily be governed by a disc.
3. Refined spin and orbital periods of 512.40 ± 0.03 s and 5.58 ± 0.01 hr, respectively, were derived using the *TESS* observations of V667 Pup. They further confirm its IP nature. However, an unambiguous beat period of 525.77 ± 0.03 s is detected for the first time in the study of this system.
4. The strong ω and 2ω frequencies suggest that V667 Pup might be accreting predominantly via the disc. The detection of a previously unknown $\omega - \Omega$ frequency indicates that part of the accreting material also directly flows towards the WD along the magnetic field lines, however.
5. The double-peaked structure with varying amplitudes observed in the optical spin pulse profile of V667 Pup suggests a possible two-pole accretion geometry, where each pole accretes at a different rate and is separated by 180° .

Acknowledgments

I thank the anonymous referee for providing useful comments and suggestions that improved the manuscript considerably. AJ acknowledges support from the Centro de Astrofísica y Tecnologías Afines (CATA) fellowship via grant Agencia Nacional de Investigación y Desarrollo (ANID), BASAL FB210003. This paper includes data collected with the *TESS* mission, obtained from the MAST data archive at the Space Telescope Science Institute (STScI). Funding for the *TESS* mission is provided by the NASA Explorer Program.

References

- Aizu, K. 1973, *Progress of Theoretical Physics*, 49, 1184
 Ajello, M., Greiner, J., Rau, A., et al. 2006, *The Astronomer's Telegram*, 697, 1

- Armitage, P. J. & Livio, M. 1996, *ApJ*, 470, 1024
 Barlow, E. J., Knigge, C., Bird, A. J., et al. 2006, *MNRAS*, 372, 224
 Buckley, D. A. H. & Tuohy, I. R. 1989, *ApJ*, 344, 376
 Butters, O. W., Barlow, E. J., Norton, A. J., & Mukai, K. 2007, *A&A*, 475, L29
 Butters, O. W., Norton, A. J., Mukai, K., & Tomsick, J. A. 2011, *A&A*, 526, A77
 Cropper, M. 1990, *Space Sci. Rev.*, 54, 195
 de Martino, D., Bernardini, F., Mukai, K., Falanga, M., & Masetti, N. 2020, *Advances in Space Research*, 66, 1209
 Evans, P. A. & Hellier, C. 2004, *MNRAS*, 353, 447
 Hameury, J.-M., King, A. R., & Lasota, J.-P. 1986, *MNRAS*, 218, 695
 Hellier, C. 1991, *MNRAS*, 251, 693
 Hellier, C. 1993, *MNRAS*, 265, L35
 Hellier, C., Mason, K. O., Smale, A. P., et al. 1989, *MNRAS*, 238, 1107
 Horne, J. H. & Baliunas, S. L. 1986, *ApJ*, 302, 757
 Kim, Y. & Beuermann, K. 1995, *A&A*, 298, 165
 King, A. R. & Lasota, J.-P. 1991, *ApJ*, 378, 674
 Littlefield, C., Garnavich, P., Kennedy, M. R., et al. 2020, *ApJ*, 896, 116
 Lomb, N. R. 1976, *Ap&SS*, 39, 447
 Lubow, S. H. 1989, *ApJ*, 340, 1064
 Marsh, T., Littlefair, S., & Dhillon, V. 2006, *The Astronomer's Telegram*, 760, 1
 Masetti, N., Bassani, L., Dean, A. J., Ubertaini, P., & Walter, R. 2006, *The Astronomer's Telegram*, 735, 1
 Murray, J. R., Armitage, P. J., Ferrario, L., & Wickramasinghe, D. T. 1999, *MNRAS*, 302, 189
 Norton, A. J., Beardmore, A. P., Allan, A., & Hellier, C. 1999, *A&A*, 347, 203
 Norton, A. J., Beardmore, A. P., & Taylor, P. 1996, *MNRAS*, 280, 937
 Norton, A. J., Hellier, C., Beardmore, A. P., et al. 1997, *MNRAS*, 289, 362
 Patterson, J. 1994, *PASP*, 106, 209
 Patterson, J., Halpern, J., Mirabal, N., et al. 2006, *The Astronomer's Telegram*, 757, 1
 Pretorius, M. L. 2009, *MNRAS*, 395, 386
 Pretorius, M. L. & Knigge, C. 2008, *MNRAS*, 385, 1471
 Rawat, N., Pandey, J. C., & Joshi, A. 2021, *ApJ*, 912, 78
 Ricker, G. R., Winn, J. N., Vanderspek, R., et al. 2015, *Journal of Astronomical Telescopes, Instruments, and Systems*, 1, 014003
 Rosen, S. R., Mason, K. O., & Cordova, F. A. 1988, *MNRAS*, 231, 549
 Scargle, J. D. 1982, *ApJ*, 263, 835
 Schwöpe, A. D. 2018, *A&A*, 619, A62
 Thorstensen, J. R. & Halpern, J. 2013, *AJ*, 146, 107
 Thorstensen, J. R., Patterson, J., Halpern, J., & Mirabal, N. 2006, *The Astronomer's Telegram*, 767, 1
 Tomsick, J. A., Chaty, S., Rodriguez, J., et al. 2006, *ApJ*, 647, 1309
 Torres, M. A. P., Steeghs, D., Garcia, M. R., et al. 2006, *The Astronomer's Telegram*, 763, 1
 Warner, B. 1986, *MNRAS*, 219, 347
 Warner, B. 1995, *Cambridge Astrophysics Series*, 28
 Wheatley, P. J., Marsh, T. R., & Clarkson, W. 2006, *The Astronomer's Telegram*, 765, 1
 Wynn, G. A. & King, A. R. 1992, *MNRAS*, 255, 83